MOLEKUL
www.jmolekul.com

Articles

https://doi.org/10.20884/1.jm.2021.16.3.804

The Influence of pH on the Nitrogen-doped TiO_2 Structure and Its Photocatalytic Activity on Methylene Blue Degradation

Cahyorini Kusumawardani*, Kristian Handoyo Sugiyarto, Anti Kolonial Prodjosantoso

[1]Department of Chemistry, Yogyakarta State University, Yogyakarta, Indonesia, 55281

*Corresponding author email: cahyorini.k@uny.ac.id

Received July 18, 2021; **Accepted** November 01, 2021; **Available online** November 15, 2021

ABSTRACT. The mesoporous nitrogen-doped titania (N-doped TiO_2) has been synthesized through sol-gel method by refluxing the precursor mixture, continued by hydrolysis process, and then followed by annealing in air at the desired temperature. The pH of precursor mixture solution before hydrolysis process has been varied to study their influence on the resulting N-doped TiO_2. The resulting material were characterized using X-Ray Diffraction (XRD), N_2 Gas Sorption Analyzer (GSA), X-ray Photoelectron Spectroscopy (XPS), Scanning Electron Microscopy (SEM), and UV Vis Spectrophotometer. The XRD analysis result showed that the pH and water content played an important role on the crystal formation of the N-doped TiO_2. The result showed that a high acidity condition resulted in a favored tendency of anatase crystalline phase, while lowering acidity leaded to the rutile formation. Porosity analysis showed the significant influence of pH in the synthesis process on the pore characteristic and pore size distribution of the resulting material. The photocatalytic activity was tested on the methylene blue degradation system comparing to pure TiO_2 and commercial Degussa P25 and the result showed that the synthesized N-doped TiO_2 provided better photocatalytic activities.

Keywords: N-doped TiO_2, one-step sol-gel, pH synthesis, photodegradation

INTRODUCTION

The photocatalytic process has been widely used to overcome the environmental problem and energy embarrassment due to its effectivity and eco-friendly. Titanium dioxide semiconductor is one of the most powerful photocatalyst materials because it has high stability, high oxidation potential, a high catalyst activity, inexpensive, nontoxic, and chemically tunable properties. However, titanium dioxide with an intrinsic band-gap energy around 3–3.4 eV, is only active in UV radiation, which only about 5% of solar energy on earth's surface, impairs TiO_2 for such important application. To overcome this limitation, it is necessary to broader the absorption edge into visible light (Pelaez et al., 2012).

Early efforts for increasing the visible light response of titanium dioxide were focused on the doping of transition metal (Basavarajappa et al., 2020; Zhou & Fu, 2013; Yu, Wang, Li, Zheng, & Cao, 2015), but several problems appeared to make metal-doped TiO_2 impractical such as thermal instability, the formation of charge carrier recombination center, and expensive facilities for ion implantation. The nonmetal doping was then found as a more effective and efficient method for utilizing TiO_2 (Shang et al., 2014; Wu, Nishikawa, Ohtani, & Chen, 2007; Yalçin et al., 2010), and among nonmetal anion doping such as N, C, S, P, nitrogen seems to be the most successful dopant for TiO_2. Synthesis N-doped TiO_2 have been widely studied, mainly prepared using annealing of TiO_2 under nitrogen atmosphere (Ryoji Asahi et al., 2014; Irie et al., 2003) and chemical proses with aqua-based such as sol-gel method (Caratto et al., 2012; Qiu and Burda, 2007; Shang et al., 2014), hydrothermal (Zhou et al., 2011), ionothermal (Pipi et al., 2017) or solvothermal (Dunnill et al., 2011). The sol-gel method is being the simple technology that does not require other nitrogen source like ammonia (Gao et al., 2014) and also it is easily controlling structure, morphology, and particle size by simple variations of synthesis parameters, such as solution pH, reactant composition, temperature, and solvent systems (Reddy et al., 2015). The formation of TiO_2 crystal and process of doping nitrogen are two processes that may occur separately (two-step) or simultaneously (one-step) depend on the applied treatment (Zhao et al., 2008).

The catalytic properties of resulted N-doped TiO_2 such as surface area, crystal structure, and porosity, are significantly influenced by parameter synthesis. In this paper, we focused on the influence of pH in the synthesis process towards the crystal structure, porosity, and catalytic activity of the resulted N-doped TiO_2. Hydrolysis reaction is main step at the synthesis process where the crystal growth and structure formation taking place, and it is highly dependent on pH to grow the crystal and to form

mesoporous structure (Cahyorini et al., 2012). Thus, it is important to obtain the optimum pH of hydrolysis process. The crystal growth is dependent on the rate of hydrolysis, as the rapid hydrolysis process tends to form rutile crystalline phase, a thermodynamically more stable crystalline phase. In this article, we report the influence of pH in the hydrolysis process on the crystal, pore, and electronic structure of N-doped TiO_2. The effect of pH on the catalyst activity of the resulting N-doped TiO_2 has also been investigated in the aqueous solution of methylene blue photodegradation under UV and the visible light radiation.

EXPERIMENTAL SECTION

Materials

Titanium tetra isopropoxide, TTIP, 97% was purchased from Aldrich. Dodecylamine 98%, was purchased from Fluka. Ethanol absolute and CH_3COOH were obtained from Merck, and methylene blue from Aldrich. All materials were used as received without purification.

Synthesis of N-doped TiO_2

The N-doped TiO_2 was synthesized as follow: a mixture of 4.7 mL dodecylamine and 80 mL of ethanol absolute was stirred for 1 hour then added by 3 mL of TTIP and then refluxed for 4 hours at 70 °C resulting a clear solution. This precursor solution was then cooled to room temperature. The pH was varied by adding different volume of CH_3COOH to the precursors solution for obtaining pH of 3.5; 5; 7; and 10. Hydrolysis process was done with the dropwise addition 25 mL of deionized water into the solution under stirring for 24 hours. After the hydrolysis process, the solution was then aged for 72 hours to result a yellowish precipitate, which was then filtered and subsequently washed using distilled water and ethanol (1/1 V/V). The nanocrystal N-doped TiO_2 was obtained by calcining the yellowish precipitate at a heating rate of 2°C/min in air atmosphere at 450°C for 4 hours.

Characterization

The crystal structure of the resulted N-doped TiO_2 powder was characterized using X-ray Powder Diffractometer (Shimadzu, X-6000) with Cu Kα radiation (λ = 0.15406 nm). The specific surface area was examined by standard BET equipment (Quantochrome Autosorb-2) and Barret-Joyner-Halenda (BJH) was used to determine the pore size distribution. The electronic structure of N-doped TiO_2 was analyzed using UV-Vis Spectrophotometer (UV-2450, Shimadzu). The elemental analysis was done using X-ray Photoelectron Spectroscopy analysis (Thermo-advantage 5200W).

Dark Adsorption Test.

The adsorption behavior of N-doped TiO_2 towards methylene blue was studied under dark condition, about 1 g calcined TiO_2 powders were solved into 10 mL of methylene blue aqueous solution with different initial concentrations and were shaken for 24 hours to achieve equilibrium. The amount of adsorbed methyl orange on the catalyst was determined by measuring the concentration of methylene blue before and after the adsorption test.

Photocatalytic Activity Test

Photocatalytic activity of the resulted catalysts was tested in the methylene blue photodegradation, by measuring the decomposition of methylene blue under UV and visible light. A 150 W high-pressure xenon arc lamp was used as the visible-light source and 150 W mercury lamp as the UV-light source. The initial concentration of methylene was 1 x 10^{-5} M and the concentrations of decomposed methylene blue were determined by measuring the absorbance at 663.5 nm with Spectronic-20.

RESULTS AND DISCUSSION

The influence of pH in the hydrolysis process on the crystal structure was analyzed using XRD and the patterns are shown in **Figure 1a**. It showed that the synthesis in acid condition (pH 3.5 and pH 5) could effectively reduce the rate of rapid hydrolysis and successfully resulted in anatase crystalline phase. However, the very high acidity condition (pH 2) is highly suppressing the hydrolysis rate and the crystal growth so that there is no crystal formed even after the annealing at 450 °C. In neutral and basic systems (pH 7 and pH 10), the hydrolysis takes place more quickly to allow the formation of the rutile crystalline phase, as indicated by the increase in the intensity of the typical rutile peak with increasing pH. The amorphous structure of the material synthesized at pH 2 was mostly changed to become rutile crystalline phase after calcined at the temperature of 600 °C (**Figure 1b**), which indicated that a very high acidity during the synthesis could effectively inhibit the anatase crystalline growth. Very high acidity caused the polymerization reaction to proceed very slowly that it is not kinetically capable of starting the formation of the crystal, even after annealing at 450 °C. However, increasing the annealing temperature to 600 °C has succeeded to result in rutile crystalline phase as also reported that calcination treatment at a minimum temperature of 600 °C, thermodynamically enables the rutile phase crystallization (Dhage et al., 2004). The crystal growth is dependent on the rate of the hydrolysis process as the rapid rate tends to form rutile crystalline phase, which is thermodynamically more stable. The high acidity condition –low pH– can reduce the rate of hydrolysis process and hydroxo-titania condensation, and also lead to the slower polymerization process, so that the formation of anatase crystal phase can take place optimally (Kartini et al., 2004). The isoelectric point of TiO_2 is in the pH range of 4.5–6.7. It means the

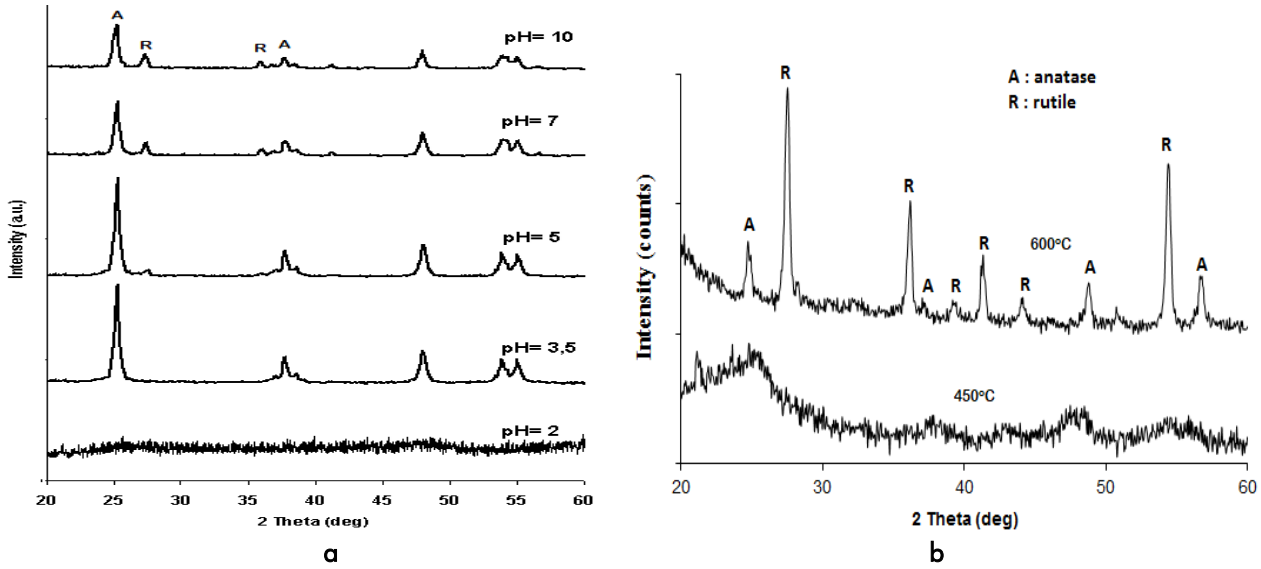

Figure 1. The diffractogram of N-doped TiO_2: (**a**). synthesized at various pH and annealed at 450 °C and (**b**) prepared at pH 2 and annealed at 450 °C and 600°C

TiO_2 surface will be very positively charged at pH less than 4.5, causing the interaction between titanium precursor and dodecylamine to become weak due to the repulsion effect and inhibiting the formation of mesoporous structure. Conversely, a pH condition at higher than 6.7 is more likely to allow strong interaction between the amine and Ti^{4+} leading to the formation of mesoporous structure (Vogel et al., 2003).

The dependence of crystal formation rate on acidity is significantly related to the speciation of precursor complexes. At pH ≤ 2, the dominant species of hydroxo- complex is in the form of $Ti(OH)_2^{2+}$, which is decreased at pH above 2 with the $Ti(OH)_3^+$ species becoming dominant. At pH above 4, the dominant species in the solution is $Ti(OH)_4$ (Sugimoto et al., 2003). The result of the synthesis showed that $Ti(OH)_3^+$ is an appropriate complex precursor of anatase crystalline phase formation in the sol-gel system so that the rate of anatase formation occurs most optimally at pH 2–4. The influence of pH on the ratio of anatase to rutile showed that the optimum pH condition to the synthesis of the anatase crystalline phase is pH 3.5 since the rutile phase started forming in the pH of ≥ 5. The higher pH on the synthesis resulted in the lower ratio of anatase to rutile crystalline phase. The crystallite sizes, which determined based on diffractogram data using Debye-Scherrer's formula, indicated that the lower acidity resulted in the lower particle size both for anatase and rutile crystalline phases (**Table 1**).

The pH of the hydrolysis process was also significantly influenced the porosity of resulted N-doped TiO_2, which was analyzed using N_2 adsorption-desorption method. The isothermic adsorption-desorption curves of N-doped TiO_2 synthesized with pH variation (**Figure 2**) indicated the isothermic type of IV with the pore size around 1-10 nm, being defined as mesoporous structure (Greg & Sing, 1982). The hysteresis curve of H2-type was defined at the materials synthesized at pH 5 and 7, it relates to the agglomerated spherical material with a narrow pore distribution. Material synthesized at pH of 3.5 showed a hysteresis curve of H4-type, indicating material with a heterogeneous pore structure and broad with wide pore size distribution. Synthesis at pH of 10 provided an H3-type hysteresis pathway, which indicated a plate-like material and a slit-shaped pore with wide pore size distribution.

Table 1. Characteristics of N-doped TiO_2

Character		pH			
		3.5	5	7	10
L	Nm	A:20.9	A:20.2 R: 24.5	A:18.9 R:22.4	A: 16.6 R: 22.1
S_{BET}	m^2g^{-1}	111.3	167.4	171.5	180.2
D_{BJH}	Nm	6.1	5.6	5.4	7.4
V_p	cm^3g^{-1}	0.137	0.236	0.241	0.318
E_g	eV	2.76	2.68	2.76	2.87

L : crystallite size, A: anatase, R: rutile
D_{BJH} : BJH pore diameter
S_{BET} : specific surface area
V_P : total pore volume
E_g : band gap energy

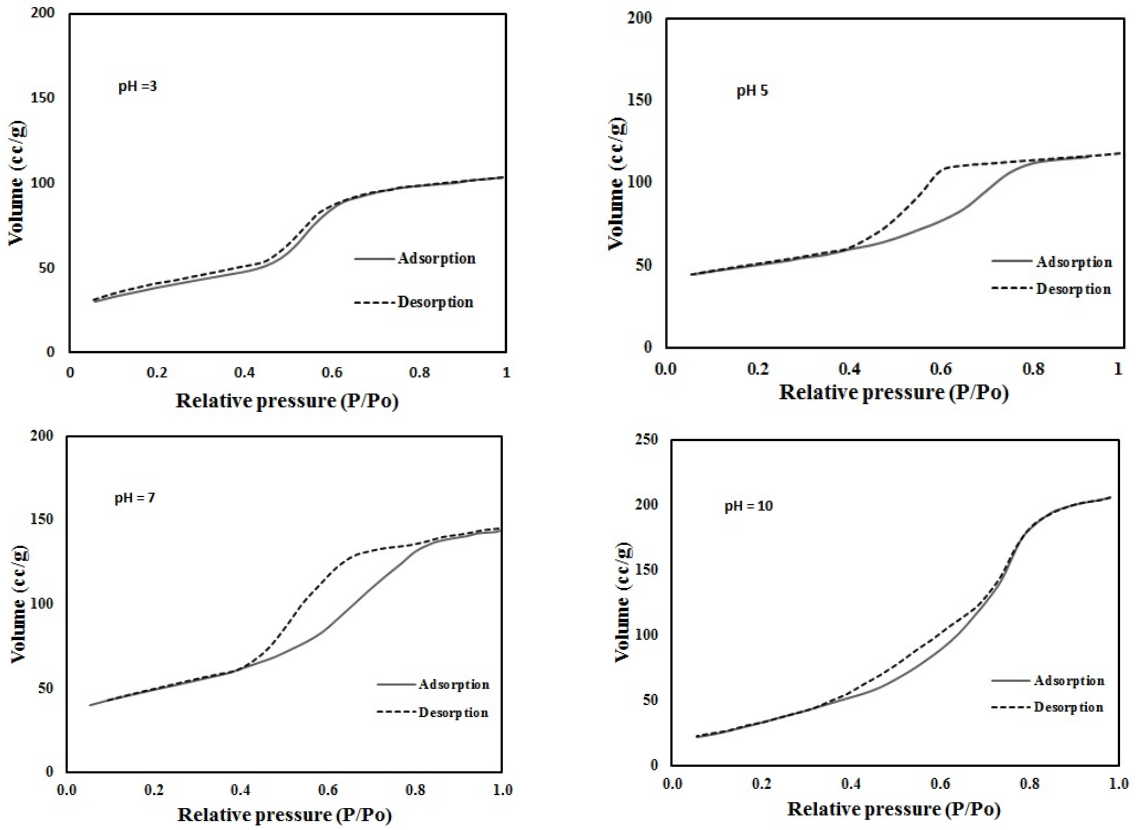

Figure 2. Isothermic adsorption-desorption curves of N-doped TiO_2 synthesized at various pH

The pore size distribution determined by the BJH desorption method is shown in **Figure 3**, indicating that a high acidity level (up to pH of 3.5) resulted in a heterogeneous pore size with a wide distribution. A decrease in acidity (down to around pH of 7) increased the pore size uniformity with the narrower peak of the pore size distribution, due to the more stable interaction between the template molecules and TiO_2 leading to a more effective mesostructured formation and reducing the occurrence of particle aggregation to form a more homogenous structure. Whereas, synthesis at pH of 10 also produced material with a wide pore size distribution, due to overly strong covalent and electrostatic bonds between the oxide and template molecules causing the collapse of the pore wall (Zhao et al., 2008). This result also found in the synthesis of silver nanoparticle, the lower pH produced a more uniform and non-agglomerated particle due to the repulsion forces and balance between the nucleation and growth steps (Alqadi et al., 2014). Wu et al. reported the same phenomena in the synthesis of zinc oxide nanostructure that decreasing pH facilitated a slower growth process and nucleation, caused by the increasing repulsion force between nanoparticle then producing a much more uniform nanoparticles with a sharper size distribution (Wu et al., 2011). The specific surface area of N-doped TiO_2, calculated from adsorption curves using BET method (listed in **Table 1**) showed that the lower acidity level leads to the increase of specific surface area.

Electronic structures of resulted materials have been analyzed using Diffuse Specular UV/Vis Spectroscopy, and the absorbance of the materials is shown in **Figure 4**. It showed that pH in the synthesis also influenced the optical character of the N-doped TiO_2 materials. The band-gap energy of the materials was calculated using Tau formation, resulted in E_g value around 2.7 – 2.9 eV (**Table 1**). The existence of nitrogen-doped in the TiO_2 framework significantly decrease the band-gap energy compared to pure TiO_2 (E_g = 3.0 – 3.4 eV), leading to the red-shift absorption edge to the visible region. In TiO_2, valence bands are formed by hybridization of 3*p*-Ti and 2*p*-O orbitals, while conduction bands are formed by empty Ti 3*d*, 4*s* and 4*p* orbitals of Ti (Ma et al., 2005). When nitrogen is bound to titanium, overlapping 2*p*-N orbitals and 2*p*-O orbitals can occur because they have the same symmetry at the t_2 level. Oxygen atoms are more electronegative than nitrogen so that the energy level of t_2 of nitrogen is slightly higher than oxygen so overlapping the t_2 level enclosed the valence band towards the conduction band. However, 2*p*-N orbitals can also hybridize with 3*d*-Ti orbitals because they have the same symmetry (t_2) at a higher energy level than the valence band of TiO_2, so a separate energy band is formed above the valence band.

Asahi *et al.* found that in the substitutional doped-nitrogen, the 2*p*-N band overlapped with 2*p*-O, so the increase in visible response and the decrease in band gap energy were caused by the joining of 2*p*-N orbitals with 2*p*-O orbitals (Ryoji Asahi et al., 2014). On the other hand, Irie *et al.* reported that based on isopropyl alcohol decomposition data, the doping nitrogen formed a unique band over the valence band of TiO_2 (Irie et al., 2003). The particle morphology of N-doped TiO_2 synthesized on pH of 5 was analyzed using SEM/EDX (**Figure 5**), which showed the spherical particle formed. The micrograph also indicated the occurrence of particle agglomeration. Elemental analysis using Energy Dispersive X-ray (EDX) confirmed the existence of nitrogen peak in the sample with overall composition of 59.2% titanium, 39.12% oxygen, and 1.63% nitrogen, being equal to Ti : O : N = 1 : 2.07 : 0.12 which means there is about 3.25% of nitrogen-doped in TiO_2.

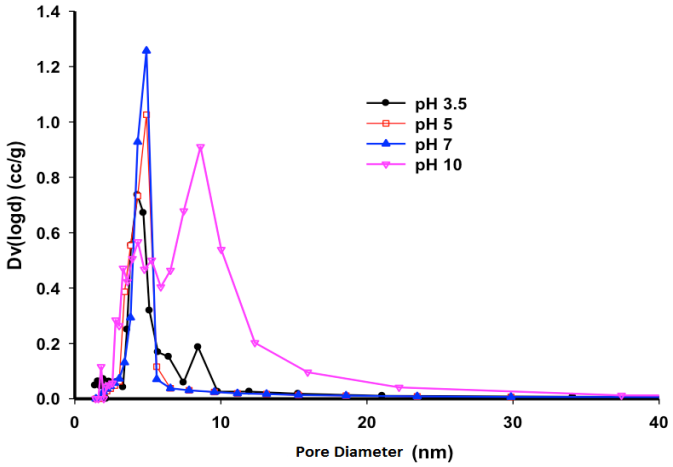

Figure 3. BJH pore size distribution of N-doped TiO_2 synthesized at various pH

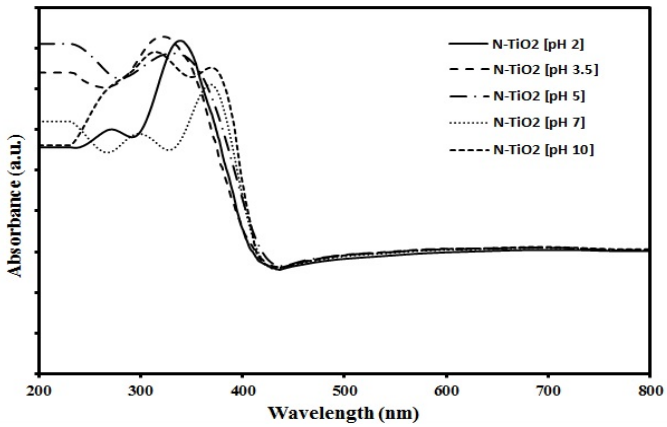

Figure 4. UV Vis Spectra of N-doped TiO_2 synthesized at various

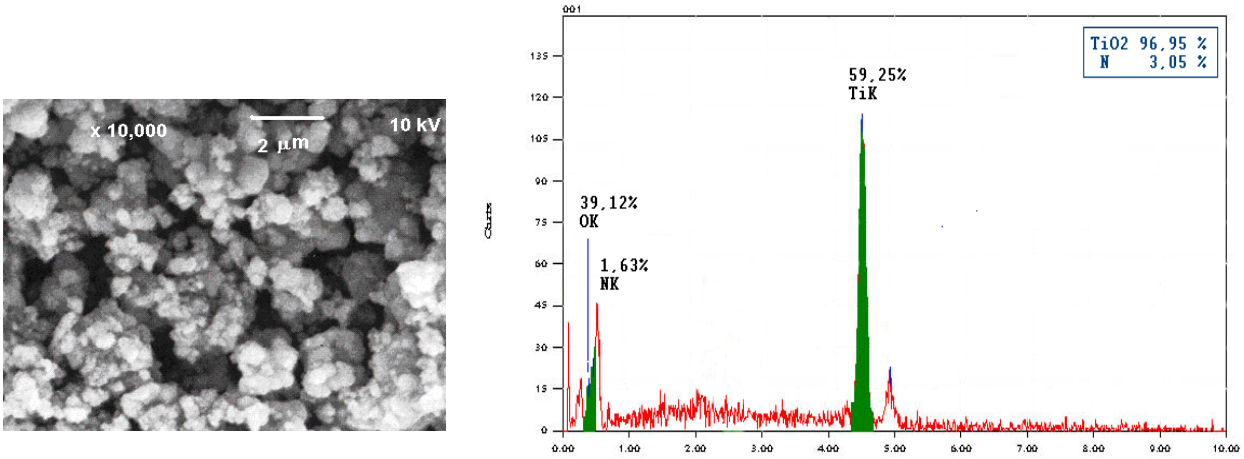

Figure 5. SEM micrograph of N-doped TiO_2 synthesized at pH 5

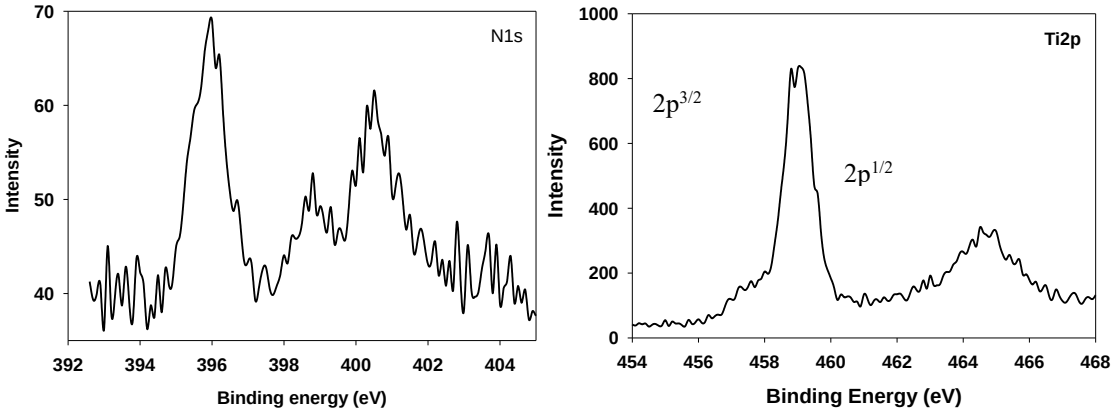

Figure 6. XPS spectra of N1s (left) and Ti2p (right) of N-doped TiO_2 calcined at 450 °C

The substitutional doped-nitrogen in the TiO_2 framework was confirmed by X-ray photoemission spectroscopy (XPS), as shown in **Figure 6**, where the 1s nitrogen core level showed three peaks at 396.0, 398.8 and 400.5 eV. The molecularly adsorbed nitrogen species were identified from the two peaks at higher binding energies, whereas the substitutionally bound N^- species was assigned from the peak at 396 eV (Lindgren et al., 2003). It was also reported that the a chemically bound N^- species was confirmed from the peak at 396 eV (Ryoji Asahi et al., 2014; Diwald, Thompson, Goralski, Walck, & Yates, 2004; Diwald, 2004; Irie et al., 2003). The N was bound into TiO_2 lattice with a 3-valence replacing O atom to form N-Ti-O bond. The doped-nitrogen such as N in the O-Ti-N linkage mostly existed as nitrides species, attributed to the binding energy (BE) of 399.4 eV, and only small amounts were present as surface adsorbed ammonia, corresponding to the BE peak located at 396.0 eV. This result are in agreement with those reported in the XPS result of N-doped TiO_2 (Boningari et al., 2018; Rangel et al., 2018; Yoshida et al., 2015). Zhang et al. found a higher N1s binding energy as the N in the N-Ti-O due to higher electronegativity of O than N leads to the higher N electron density in the N-Ti-O structure than that of N in the N-Ti-N structure (Zhang et al., 2015). In the $Ti2p^{3/2}$ XPS spectra, the major titanium peak is centered at 459 eV and the Ti-N bound was assigned from an intermediate peak at ca. 457.5 eV. The XPS elemental analysis confirmed about 3.6% nitrogen doped on TiO_2, which is higher than that confirmed by EDX data since the EDX only counted the nitrogen on the surface.

Photocatalytic Activity

The process of photocatalytic reactions using a porous-solid catalyst usually occurs on the catalyst surface so adsorption plays an important role in the reaction mechanism. Therefore, it was a need to study the adsorption properties of the catalyst towards methylene blue, which have been determined using dark adsorption method for 24 hours. The prepared N-doped TiO_2 photocatalytic activity has been compared to pure TiO_2 and commercial Degussa P25, and pure titania was synthesized without the use of dodecylamine at pH 5. Based on the porosity data, the adsorption properties could be analyzed using the Langmuir adsorption isotherm equation. By plotting equilibrium concentration of methylene blue in the solution (*c*) versus amount of adsorbed methylene blue for every 1 g catalyst (*m*), it can be defined the Langmuir adsorption pattern for every catalyst (**Figure 7**).

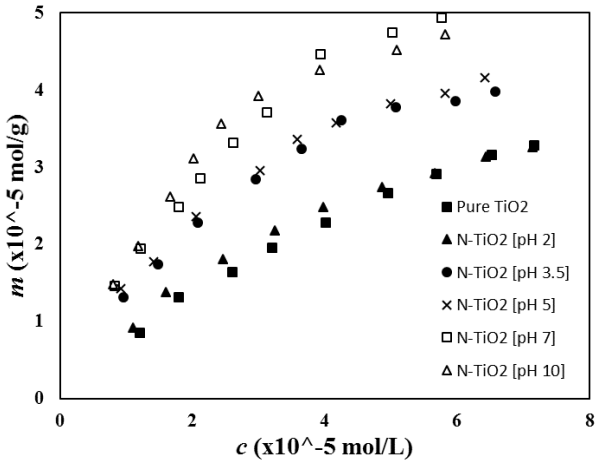

Figure 7. Adsorption isothermic curves of N-doped TiO_2 synthesized at various pH

Table 2. Adsorption character of the synthesized N-doped TiO_2 towards MB

Catalyst	b x 10^{-5} (mol g^{-1})	K_L x 10^2 (L mol^{-1})	r^2
Pure TiO_2	3.87	2.09	0.9826
N-TiO_2 [pH 2]	3.85	2.08	0.9802
N-TiO_2 [pH 3.5]	5.38	4.43	0.9783
N-TiO_2 [pH 5]	5.42	4.59	0.9632
N-TiO_2 [pH 7]	5.68	4.54	0.9912
N-TiO_2 [pH 10]	5.82	4.46	0.9816

From the curve of c/m versus c, the maximum adsorption capacity (b) can be determined from the intercept and equilibrium adsorption constant derived from the slope (the data listed in **Table 2**), showed that N-doped TiO_2 catalysts (except N-doped TiO_2 synthesized at pH 2) have a better adsorption capacity compared to pure titania, with the value of the adsorption capacity and the adsorption constant equilibrium at least 1.5 times. The increase in adsorption character with the increase of pH is related to the changes in the physical properties of the catalyst such as specific surface area, crystalline phase, and pore diameter size.

The kinetic study of methylene blue photodegradation was examined as a comparison of concentration changes to understand the nature of adsorption process in the degradation reaction under visible and UV light sources. The kinetic curve of MB photodegradation with visible radiation depicted in Figure 8, which showed that N-doped TiO_2 degraded MB faster than pure TiO_2 and Degussa P25. As in the visible region, N-doped TiO_2 also has better activity than pure TiO_2 in the UV region, although it is still lower than Degussa P25. This is related to the intensity of absorption of UV light in the region <800 nm, which is higher than TiO_2 synthesized. Based on the kinetic curves with visible and UV sources, it can be seen that the rate of photodegradation in the UV region is higher than that in the visible region because in the UV region the equilibrium is achieved faster than in the visible region. In general, it is also seen that catalysts with greater adsorption capacity and adsorption equilibrium constants have better activity as MB photodegradation catalysts. This means that the adsorption process is an important part of the photocatalysis process.

The dependence of MB photodegradation reaction rate using TiO_2 catalyst on the concentration of organic reactant, showed that the reaction tendency follows a pseudo first-order reaction (Liu et al., 2005). Therefore, the use of the Langmuir-Hinshelwood (L-H) kinetic reaction model is more appropriate to describe the MB photodegradation reaction with the synthesized N-doped TiO_2 catalyst in this study. K_{obs} kinetic constant is an observed reaction rate constant that does not take the role of adsorption into account, so when the adsorption process becomes a significant part of the photodegradation reaction it is necessary to determine the actual reaction rate by excluding the adsorption process. The reaction rate constant (k) determined based on k_{obs} and the results are presented in **Table 3**.

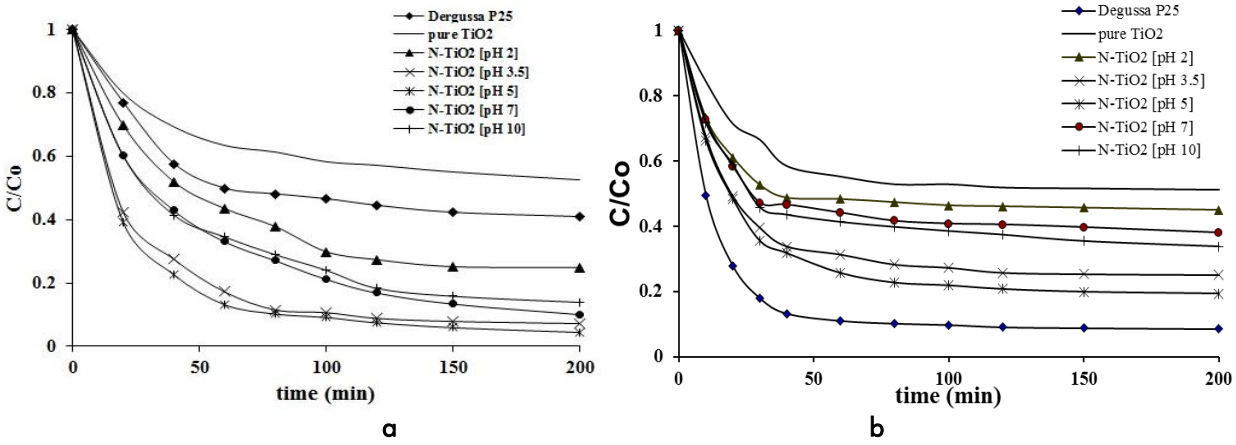

Figure 8. Kinetic curve of methylene blue photodegradation with the synthesized catalyst under (**a**) visible and (**b**) UV light

Table 3. The kinetic data of MB photodegradation with N-doped TiO_2 under visible and UV light

catalyst	k_{obs} (min^{-1})	K_{obs} N-TiO_2/ k_{obs} TiO_2	R^2	k (min^{-1})	k N-TiO_2/ k TiO_2
Visible light					
Degussa P25	0.117	1.62			
Pure titania	0.073	1.00	0.9717	0.0035	1.00
N-TiO_2 [pH 2]	0.105	1.43	0.9688	0.0050	1.48
N-TiO_2 [pH 3.5]	0.372	5.09	0.9896	0.0084	2.40
N-TiO_2 [pH 5]	0.336	4.61	0.9912	0.0079	2.26
N-TiO_2 [pH 7]	0.302	4.02	0.9824	0.0066	1.89
N-TiO_2 [pH 10]	0.278	3.81	0.9779	0.0063	1.81
UV light					
Degussa P25	0.506	3.72	0.9763		
Pure titania	0.136	1.00	0.9797	0.0065	1.00
N-TiO_2 [pH 2]	0.192	1.42	0.9636	0.0079	1.31
N-TiO_2 [pH 3.5]	0.442	3.25	0.9685	0.0099	1.52
N-TiO_2 [pH 5]	0.426	3.13	0.9861	0.0093	1.43
N-TiO_2 [pH 7]	0.328	2.41	0.9874	0.0074	1.14
N-TiO_2 [pH 10]	0.325	2.39	0.9902	0.0075	1.15

Degussa P25 is a catalyst commonly used as a test standard for TiO_2-based photocatalyst activity, especially with UV light sources. Therefore, Degussa P25 has the best activity in MB photodegradation reaction with UV photon sources. However, in the visible area the Degussa P25 activity is lower than N-doped TiO_2 activities. Table 3 showed that all N-doped TiO_2 provides a better performance in MB photodegradation than pure TiO_2 in the visible and UV regions. In the visible region, the constant rate of the observed reaction (k_{obs}) with N-doped TiO_2 catalysts is higher than pure TiO_2, with N-doped TiO_2 [pH 3.5] giving the highest value. After taking account of adsorption factor of MB desorption on the catalyst, the actual reaction rate constant (k) values indicated that the adsorption character significantly influenced the photoactivity of the catalyst which can be seen from decreasing the ratio of k N-doped TiO_2 towards k TiO_2. However, there was only slightly difference in the actual reaction rate (k) of the catalysts, which performed under UV light. Thus, it can be said that the existence of nitrogen doping significantly increases the activity of catalyst in MB degradation reaction. It was reported that the doped-nitrogen not only enhanced the visible-light photocatalytic activity by altering the electronic structure of TiO_2 but also reducing the recombination of e^-/h^+ (Siuzdak et al., 2015). The higher photoactivity with the existence of nitrogen doping have been reported in many photocatalytic systems (Ansari et al., 2016; Caratto et al., 2012; Lusvardi et al., 2017; Ruzmanova et al., 2015; Siuzdak et al., 2015).

The relation between physical properties or prepared N-doped TiO_2 towards photocatalytic activity showed that surface area has significant affected to the observed reaction rate constant (k_{obs}), the catalyst with a higher surface area and particle size has a higher value of k_{obs}. It indicated that adsorption process is being an important part in the overall photocatalytic reaction. While, the actual reaction rate constant (k) data showed that catalyst with higher ratio anatase to rutile crystalline phase has a higher reaction rate constant, means that the degradation of methylene blue by the N-doped TiO_2 catalyst was more proportional to the crystalline phase than other physical properties such as surface area and particle size. These phenomena have also been reported in the methylene blue decomposition under black light, which proportional to the mass fraction of anatase (Ansari et al., 2016; Jang et al., 2001).

CONCLUSIONS

The N-doped TiO_2 has been synthesized through one-step sol-gel method under various pH to study the influence of acidity towards the crystal structure, porosity, electronic structure, and photocatalyst activity in methylene blue photodegradation. The pH in the synthesis significantly influenced the crystalline phase, the higher acidity condition facilitating a better anatase phase formation. The porosity character also is highly dependent the acidity condition, where the synthesis at pH of 5 is being the optimum condition to form mesoporous structure. The acidity change also provide effect on the electronic structure with the red-shift absorption edge resulted in band-gap energy at around 2.8 eV. The activity test showed that the acidity directly influenced the physical character such as surface area and crystalline phase, which is directly affect the adsorption character and photocatalyst activity in methylene blue photodegradation.

ACKNOWLEDGEMENTS

Financial Support from Indonesian Government granted by Directorate General of Higher Education is gratefully acknowledged.

REFERENCES

Alqadi, M. K., Abo Noqtah, O. A., Alzoubi, F. Y., Alzouby, J., & Aljarrah, K. (2014). PH effect on the aggregation of silver nanoparticles synthesized by chemical reduction. *Materials Science- Poland*, *32*(1), 107–111. https://doi.org/10.2478/s13536-013-0166-9

Ansari, S. A., Khan, M. M., Ansari, M. O., & Cho, M. H. (2016). Nitrogen-doped titanium dioxide (N-doped TiO_2) for visible light photocatalysis. *New Journal of Chemistry*, *40*(4), 3000–3009. https://doi.org/10.1039/c5nj03478g

Asahi, R, Morikawa, T., Ohwaki, T., Aoki, K., & Taga, Y. (2001). Visible-light photocatalysis in nitrogen-doped titanium oxides. *Science (New York, N.Y.)*, *293*, 269–271. https://doi.org/10.1126/science.1061051

Asahi, Ryoji, Morikawa, T., Irie, H., & Ohwaki, T. (2014). Nitrogen-doped titanium dioxide as visible-light-sensitive photocatalyst: Designs, developments, and prospects. *Chemical Reviews*, *114*(19), 9824–9852. https://doi.org/10.1021/cr5000738

Basavarajappa, P. S., Patil, S. B., Ganganagappa, N., Reddy, K. R., Raghu, A. V., & Reddy, C. V. (2020). Recent progress in metal-doped TiO2, non-metal doped/codoped TiO_2 and TiO_2 nanostructured hybrids for enhanced photocatalysis. *International Journal of Hydrogen Energy*, *45*(13), 7764–7778. https://doi.org/10.1016/j.ijhydene.2019.07.241

Boningari, T., Inturi, S. N. R., Suidan, M., & Smirniotis, P. G. (2018). Novel one-step synthesis of nitrogen-doped TiO_2 by flame aerosol technique for visible-light photocatalysis: Effect of synthesis parameters and secondary nitrogen (N) source. *Chemical Engineering Journal*, *350*, 324–334. https://doi.org/10.1016/j.cej.2018.05.122

Cahyorini, K., Suwardi, Indriana, K., & Narsito. (2012). Synthesis and characterization of visible-light active nitrogen-doped TiO_2 photocatalyst. *Asian Journal of Chemistry*, *24*(1).

Cao, Y., Tan, H., Shi, T., Tang, T., & Li, J. (2008). Preparation of Ag-doped TiO_2 nanoparticles for photocatalytic degradation of acetamiprid in water. *Journal of Chemical Technology and Biotechnology*, *83*, 546–552.

Caratto, V., Setti, L., Campodonico, S., Carnasciali, M. M., Botter, R., & Ferretti, M. (2012). Synthesis and characterization of nitrogen-doped TiO_2 nanoparticles prepared by sol-gel method. *Journal of Sol-Gel Science and Technology*, *63*(1), 16–22. https://doi.org/10.1007/s10971-012-2756-0

Dhage, S., Gaikwad, S., & Ravi, V. (2004). Synthesis of nanocrystalline TiO_2 by tartrate gel method. *Bulletin of Materials Science - BULL MATER SCI*, *27*, 487–489. https://doi.org/10.1007/BF02707273

Diwald, O., Thompson, T. L., Goralski, E. G., Walck, S. D., & Yates, J. T. (2004). The effect of nitrogen ion implantation on the photoactivity of TiO_2 rutile single crystals. *Journal of Physical Chemistry B*, *108*(1), 52–57. https://doi.org/10.1021/jp030529t

Diwald, O., Thompson, T. L., Zubkov, T., Goralski, E. G., Walck, S. D., & Yates, J. T. (2004). Photochemical activity of nitrogen-doped rutile TiO_2(110) in visible light. *Journal of Physical Chemistry B*, *108*(19), 6004–6008. https://doi.org/10.1021/jp031267y

Dunnill, C. W., Ansari, Z., Kafizas, A., Perni, S., Morgan, D. J., Wilson, M., & Parkin, I. P. (2011). Visible light photocatalysts - N-doped TiO_2 by sol-gel, enhanced with surface bound silver nanoparticle islands. *Journal of Materials Chemistry*, *21*(32), 11854–11861. https://doi.org/10.1039/c1jm11557j

Gao, Y., Feng, Y., Zhang, B., Zhang, F., Peng, X., Liu, L., & Meng, S. (2014). Double-N doping: A new discovery about N-doped TiO_2 applied in dye-sensitized solar cells. *RSC Advances*, *4*(33), 16992–16998. https://doi.org/10.1039/c4ra00053f

Greg, S. J., & Sing, K. S. W. (1982). *Adsorption, surface area, and porosity* (2nd ed.). Academic Press.

Irie, H., Watanabe, Y., & Hashimoto, K. (2003). Nitrogen-concentration dependence on photocatalytic activity of $TiO_{2-x}N_x$ powders. *Journal of Physical Chemistry B*, *107*(23), 5483–5486.

Jang, H. D., Kim, S.-K., & Kim, S.-J. (2001). Effect of particle size and phase composition of titanium dioxide nanoparticles on the photocatalytic properties. *Journal of Nanoparticle Research*, *3*, 141–147.

Kartini, I., Meredith, P., Da Costa, J. C. D., & Lu, G. Q. (2004). A novel route to the synthesis of mesoporous titania with full anatase nanocrystalline domains. *Journal of Sol-Gel Science and Technology*, *31*(1-3 SPEC.ISS.), 185–189. https://doi.org/10.1023/B:JSST.0000047984.60654.al

Lindgren, T., Mwabora, J. M., Avandaño, E., Jonsson, J., Hoel, A., Granqvist, C. G., & Lindquist, S. E. (2003). Photoelectrochemical and optical properties of nitrogen doped titanium dioxide films prepared by reactive DC magnetron sputtering. *Journal of Physical Chemistry B*, *107*(24), 5709–5716.

https://doi.org/10.1021/jp027345j

Liu, Y., Chen, X., Li, J., & Burda, C. (2005). Photocatalytic degradation of azo dyes by nitrogen-doped TiO_2 nanocatalysts. *Chemosphere*, *61*(1), 11–18. https://doi.org/10.1016/j.chemosphere.2005.03.069

Lusvardi, G., Barani, C., Giubertoni, F., & Paganelli, G. (2017). Synthesis and characterization of TiO_2 nanoparticles for the reduction of water pollutants. *Materials*, *10*(10), 1–11. https://doi.org/10.3390/ma10101208

Ma, T., Akiyama, M., Abe, E., & Imai, I. (2005). High-efficiency dye-sensitized solar cell based on a nitrogen-doped nanostructured titania electrode. *Nano Letters*, *5*(12), 2543–2547. https://doi.org/10.1021/nl051885l

Pelaez, M., Nolan, N. T., Pillai, S. C., Seery, M. K., Falaras, P., Kontos, A. G., Dunlop, P. S. M., Hamilton, J. W. J., Byrne, J. A., O'Shea, K., Entezari, M. H., & Dionysiou, D. D. (2012). A review on the visible light active titanium dioxide photocatalysts for environmental applications. *Applied Catalysis B: Environmental*, *125*, 331–349. https://doi.org/10.1016/j.apcatb.2012.05.036

Pipi, A., Byzynski, G., & Ruotolo, L. (2017). Photocatalytic activity and RNO dye degradation of nitrogen-doped TiO_2 prepared by ionothermal synthesis. *Materials Research*, *20*(3), 628–638. https://doi.org/10.1590/1980-5373-MR-2016-0837

Qiu, X., & Burda, C. (2007). Chemically Synthsized Nitrogen-doped Metal Oxide nanoparticles. *Chemical Physiscs*, *339*(1–3), 1–10.

Rangel, R., Cedeño, V. J., Espino, J., Bartolo-Pérez, P., Rodríguez-Gattorno, G., & Alvarado-Gil, J. J. (2018). Comparing the efficiency of N-doped TiO_2 and N-doped bi_2 MoO_6 photo catalysts for MB and lignin photodegradation. *Catalysts*, *8*(12). https://doi.org/10.3390/catal8120668

Reddy, K. R., Hassan, M., & Gomes, V. G. (2015). Hybrid nanostructures based on titanium dioxide for enhanced photocatalysis. *Applied Catalysis A: General*, *489*, 1–16. https://doi.org/10.1016/j.apcata.2014.10.001

Ruzmanova, Y., Stoller, M., Bravi, M., & Chianese, A. (2015). A novel approach for the production of nitrogen doped TiO_2 nanoparticles. *Chemical Engineering Transactions*, *43*, 721–726. https://doi.org/10.3303/CET1543121

Shang, X., Zhang, M., Wang, X., & Yang, Y. (2014). Sulphur, nitrogen-doped TiO_2/graphene oxide composites as a high performance photocatalyst. *Journal of Experimental Nanoscience*, *9*(7), 749–761. https://doi.org/10.1080/17458080.2012.713127

Siuzdak, K., Szkoda, M., Sawczak, M., & Lisowska-Oleksiak, A. (2015). Novel nitrogen precursors for electrochemically driven doping of titania nanotubes exhibiting enhanced photoactivity. *New Journal of Chemistry*, *39*(4), 2741–2751.

Sugimoto, T., Zhou, X., & Muramatsu, A. (2003). Synthesis of uniform anatase TiO_2 nanoparticles by gel-sol method: 3. Formation process and size control. *Journal of Colloid and Interface Science*, *259*(1), 43–52. https://doi.org/10.1016/S0021-9797(03)00036-5

Umebayashi, T., Yamaki, T., Tanaka, S., & Asai, K. (2003). Visible light-induced degradation of methylene blue on S-doped TiO_2. *Chemistry Letters*, *32*(4), 330–331. https://doi.org/10.1246/cl.2003.330

Vogel, R., Meredith, P., Kartini, I., Harvey, M., Riches, J. D., Bishop, A., Heckenberg, N., Trau, M., & Rubinsztein-Dunlop, H. (2003). Mesostructured dye-doped titanium dioxide for micro-optoelectronic applications. *ChemPhysChem*, *4*(6), 595–603. https://doi.org/10.1002/cphc.200200494

Wu, G., Nishikawa, T., Ohtani, B., & Chen, A. (2007). Synthesis and characterization of carbon-doped TiO_2 nanostructures with enhanced visible light response. *Chemistry of Materials*, *19*(18), 4530–4537. https://doi.org/10.1021/cm071244m

Wu, W. Y., Kung, W. Y., & Ting, J. M. (2011). Effect of pH values on the morphology of zinc oxide nanostructures and their photoluminescence spectra. *Journal of the American Ceramic Society*, *94*(3), 699–703. https://doi.org/10.1111/j.1551-2916.2010.04146.x

Yalçin, Y., Kiliç, M., & Çinar, Z. (2010). The role of non-metal doping in TiO_2 photocatalysis. *Journal of Advanced Oxidation Technologies*, *13*(3), 281–296. https://doi.org/10.1515/jaots-2010-0306

Yoshida, T., Niimi, S., Yamamoto, M., Ogawa, S., Nomoto, T., & Yagi, S. (2015). Characterization of nitrogen ion implanted TiO_2 photocatalysts by XAFS and XPS. *Nuclear Instruments and Methods in Physics Research, Section B: Beam Interactions with Materials and Atoms*, *365*, 79–81. https://doi.org/10.1016/j.nimb.2015.04.010

Yu, Y., Wang, J., Li, W., Zheng, W., & Cao, Y. (2015). Doping mechanism of Zn^{2+} ions in Zn-doped TiO_2 prepared by sol-gel method. *CrystEngComm*, *17*. https://doi.org/10.1039/C5CE00933B

Zhang, X., Zhou, J., Gu, Y., & Fan, D. (2015). Visible-light photocatalytic activity of N-poped TiO_2 nanotube arrays on acephate degradation. *Journal of Nanomaterials*, *2015*. https://doi.org/10.1155/2015/527070

Zhao, L., Jiang, Q., & Lian, J. (2008). Visible-light photocatalytic activity of nitrogen-doped TiO_2

thin film prepared by pulsed laser deposition. *Applied Surface Science*, *254*(15), 4620–4625. https://doi.org/10.1016/j.apsusc.2008.01.069

Zhou, X., Peng, F., Wang, H., Yu, H., & Yang, J. (2011). Preparation of nitrogen doped TiO_2 photocatalyst by oxidation of titanium nitride with H_2O_2. *Materials Research Bulletin*, *46*(6), 840–844. https://doi.org/10.1016/j.materresbull.2011.02.029